Occupied-Virtual Orbitals for Chemical Valence with Applications to Charge Transfer in Energy Decomposition Analysis.

Hengyuan Shen and Martin Head-Gordon*

Pitzer Center for Theoretical Chemistry, Department of Chemistry, University of California, Berkeley, California 94720, USA

E-mail: mhg@cchem.berkeley.edu

Abstract

In this article, we introduce the occupied-virtual orbitals for chemical valence (OVOCV). The OVOCVs can replace or complement the closely related idea of the natural orbitals for chemical valence (NOCV). The input is a difference density matrix connecting any initial single determinant to any final determinant, at a given molecular geometry, and a given one-particle basis. This arises in problems such as orbital rearrangement or charge-transfer in energy decomposition analysis. The OVOCVs block-diagonalize the density difference operator into 2×2 blocks which are spanned by one level that is filled in the initial state (the occupied OVOCV) and one which is empty (the virtual OVOCV). By contrast, the NOCVs fully diagonalize the density difference matrix, and therefore are orbitals with mixed occupied-virtual character. Use of the OVOCVs makes it much easier to identify the donor and acceptor orbitals. We also introduce two different types of energy decomposition analysis (EDA) methods with the OVOCVs, and most importantly, a charge decomposition analysis (CDA) method that fixes the unreasonably large charge transfer amount obtained directly from NOCV analysis. The square of the charge transfer amount associated with each NOCV pair emerges as the appropriate value from the OVOCV analysis. When connecting the same initial and final states, this value is identical to the CT amount obtained from the independent absolutely localized molecular orbital (ALMO) complementary occupied-virtual orbital pair (ALMO-COVP) analysis. The total, summed over all pairs, is also exactly the same as the independently suggested excitation number, as proved herein. Several examples are presented to compare NOCVs and OVOCVs: stretched H₂⁺, a strong halogen bond between tetramethylthiourea and iodine, coordination of ethene in Zeise's salt, and binding in the $Cp_3 La \cdots C \equiv NCy$ complex.

Introduction

Electron donor-acceptor interactions have long been recognized by chemists as a heuristic and powerful concept to understand the chemistry of substances. Even before the popular application of quantum mechanics to chemistry, G. N. Lewis has provided his famous definition^{1,2} of acid and base as the acceptor and donor of an electron pair, respectively. In the field of coordination chemistry, Sidgwick³ also noticed that the formation of classical coordination complexes is generally a result of donation of the electron pairs from the ligands to the transition metal. Later, this evolved to the famous Dewar-Chatt-Duncanson model⁴⁵ which describes the bonding of transition metal complexes as a synergic process of electron donation from the ligands to metal and back-donation from metal to the ligands. While these ideas have tremendous qualitative value, a deeper understanding of electron donation can be achieved by examining the involved donor and acceptor orbitals with the help of quantum mechanics, as they are able to provide more information on the direction of the electron donation. For example, to explain the chemisorption of CO on metal surfaces, the widely accepted Blyholder model⁶ proposes the bonding of CO to the metal surface as a result of the donation from the 5σ orbital of CO to metal and back donation from metal to the 2π orbital of CO.

However, since electron donation is a useful chemical concept without a well-defined physical observable and orbitals are only effective one-electron building blocks of the many-electron wavefunction, there is no unique way to obtain the electron donor-acceptor orbitals using quantum mechanics. Fortunately, the development of computational quantum chemistry has provided us with many useful methods to get reasonable and intuitive donor-acceptor orbitals, as well as more insights into their significance from the associated energy decrease and the amount of transferred charge with the help of energy decomposition analysis (EDA) and charge decomposition analysis (CDA).^{7–9} Examples of some successful and popular orbital methods are natural bonding orbitals (NBO),^{10,11} natural orbitals for chemical valence (NOCV)^{12,13} and complementary occupied-virtual pairs (COVP).^{14–16} In addition,

it is important to keep in mind that these donor-acceptor orbitals describe the formation of ground state complexes or bonds from individual fragments, and they should not be confused with donor-acceptor orbitals that describe electron transitions between different electronic states, such as natural transition orbitals (NTO).¹⁷

The NOCV method is one of the most popular orbital methods used to understand and analyse chemical bonding and donor-acceptor interactions. The NOCVs are obtained from diagonalizing the density difference operator, which is the subtraction of the density operators of the initial fragment-sum state and the final converged state from a self-consistent field (SCF) calculation.¹² This is identical to evaluating and diagonalizing the attachment and detachment density matrices that connect initial and final states.¹⁸ At the SCF level, the eigenvalues are strictly paired, ¹⁶ positive and negative, σ_{\pm} , with typically only a few σ being significantly non-zero. The resulting picture of bonding for each significant eigenvalue σ is:

$$\Delta \rho_{\sigma} = |\psi_{-}|^2 \to |\psi_{+}|^2 \tag{1}$$

Either the orbitals ψ_{\pm} or the change in density, $\Delta \rho_{\sigma}$ can be visualized. Combined with the extended transition state (ETS) method, ^{19–21} the ETS-NOCV method ²² provides both the charge contribution and the energy contribution for the electron donation process, as well as a readily visualized set of orbitals or density changes corresponding to those contributions. As a result, the ETS-NOCV method has a wide application in analysing chemical bonding, ranging from very general studies ⁷ to specific examples such as metal-ligand bonds, ^{23,24} metal-metal bonds, ²⁵ hydrogen bonds, ^{26,27} halogen bonds ²⁸ and boron bonds. ²⁹ It has also been used to study chemical reactions ^{30–32} and concerted transition states. ³³

However, the NOCVs are generally delocalized over all fragments and it can be hard to recognize the fragment character of the orbitals. Thus, density difference plots of NOCVs are often used to show the direction of electron transfer, at the price of losing the phase information of the orbitals. As a simple example, Figure 1 shows the plots of the most significant NOCV pair for the CT process of $(H_2O)_3$ (there are another 2 NOCV pairs with similar

but smaller energy contributions). It is obvious that the NOCVs are describing formation of one of the hydrogen bonds, with ψ_1 showing constructive interference along an $H_2O \cdots HOH$ distance, and ψ_{-1} showing destructive interference. However $\psi_{\pm 1}$ are delocalized across two H_2O molecules and one cannot recognize the donor and acceptor orbitals from the NOCV plots directly. By contrast, the density difference, $\Delta \rho_1$, indicates that electrons flow from the H_2O molecule on the left (negative red lobe) to the H_2O molecule on the right (positive blue lobe), and the shape of the density suggests a donation from the oxygen lone pair to the σ^* anti-bonding orbital of the OH bond. However, the recognition of donor-acceptor orbitals are helped with our chemical intuition for this simple system, and as the density difference plot offers no phase information, the identification of orbitals can be hard for complex systems where our chemical intuition is limited.

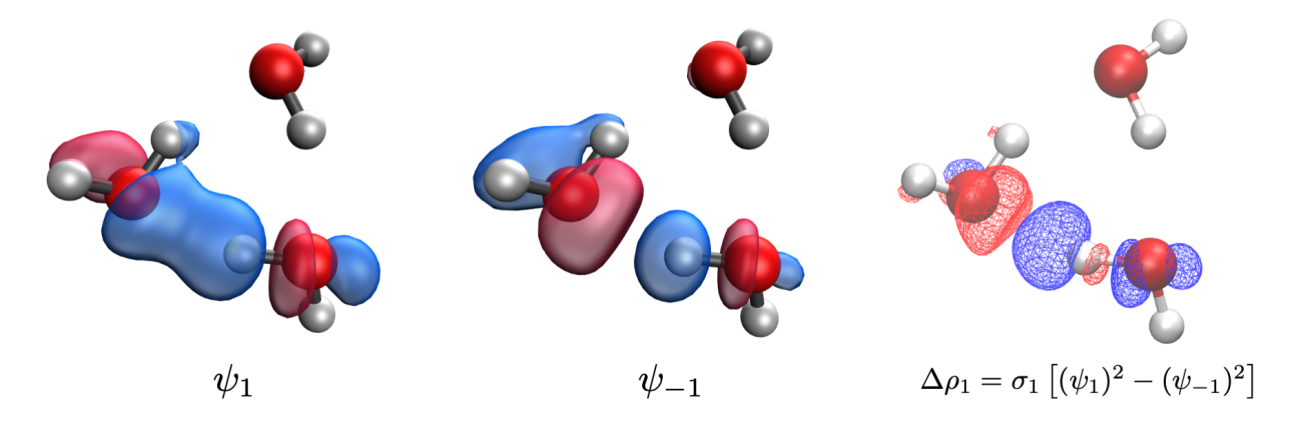


Figure 1: Plots of the most significant NOCV orbital pair, and the NOCV density difference for the CT process in a $(H_2O)_3$ cluster. The CT-free state is optimized by SCF-MI, 34,35 as in the ALMO-EDA, 8,36 while the CT-containing final state is unconstrained SCF. The calculations are at the ω B97X-D/aug-cc-pVTZ level of theory. 37,38 The NOCV plots are with an isosurface value of ± 0.07 a.u. The NOCV density difference plot is at an isosurface value of $\pm 3 \times 10^{-4}$ a.u.

There is also a second well-known limitation of the standard NOCV analysis. Specifically, a naive use of the NOCV eigenvalues tends to greatly overestimate the associated amount of transferred charge. $^{39-41}$ This can be clearly seen for the simple model 16 of forming $\rm H_2^+$ from $\rm H^+$ and $\rm H$ at long distance. While $0.5~e^-$ should be transferred from $\rm H$ to $\rm H^+$ to form the one-electron chemical bond, the NOCV eigenvalues instead suggests that $0.71~e^-$ are

transferred which is impossible. Using the NOCV eigenvalues leads to overestimated charge transfer because they measure electron transfer from one NOCV orbital to its paired partner orbital (Eqn. 1). However, the NOCV orbitals are inherently delocalized, and mix orbitals that are filled and empty in the initial state. For instance Figure 1 shows a clear contribution of the acceptor OH σ^* orbital to both ψ_1 and ψ_{-1} . Likewise the donor lone O pair orbital contributes to both ψ_{-1} and ψ_1 . Therefore these eigenvalues cannot be easily associated with charge transfer between two fragments or the number of electrons rearranged between initial and final state. Since the NOCV analysis is identical to attachment-detachment analysis ¹⁸ in the case of initial and final single determinant states, a similar caution applies there. Efforts have been made to generate improved estimates of numbers of electrons rearranged in NOCV analysis, ⁴² drawing on charge-displacement analysis of the real space difference density. ³⁹ A very useful "excitation number" was also introduced for single determinant initial and final states ⁴³ which will directly connect to the new analysis here.

The purpose of this paper is to introduce a slight, but important modification of the NOCV procedure to provide a correct and meaningful estimation of the number of electrons transferred or promoted on the one hand, and on the other hand to provide orbitals that are easier to chemically interpret. The resulting occupied-virtual orbitals for chemical valence (OVOCV) do not completely diagonalize the density difference operator: they just diagonalize it into 2 × 2 blocks corresponding to each OVOCV pair. As a result, the OVOCVs are much less delocalized than the NOCVs, making it easier to recognize the involved donor and acceptor orbitals. In addition, the OVOCVs give more reasonable amount of transferred charge. Interestingly, we will show this value is exactly the same as that obtained from the absolutely localized molecular orbital with complementary occupied-virtual pairs (ALMOCOVP) method ^{15,16} between the same initial and final states. We shall show that the sum of these values is also exactly the same as the excitation number. ⁴³ Though this is a general theory between any two single determinant electronic states, we limit our analysis to the charge transfer (CT) process in forming molecular complexes, since this eliminates the po-

larization effect and makes the donor-acceptor orbitals more obvious, while the polarization process can be analysed with COVPs⁴⁴ if desired.

The remainder of this paper is organized as follows. The detailed construction of OVOCVs is described in Sec. after a heuristic review of the construction of COVPs, and followed by the comparison with the NOCVs. Application of OVOCV in ALMO and ETS EDA frameworks is also discussed. We then show a series of examples to demonstrate the usefulness of the OVOCVs. We first show the simple toy model of H – H⁺, where the amount of transferred charge is wrong in NOCV, but is fixed here with OVOCV. We then show the CT analysis for a strong halogen-bonding system, the tetramethylthiourea-iodine cluster, whose electron donation process is also succinctly revealed. Finally, we analyse the bonding process of the classical Zeise's salt, where the OVOCVs reveal exactly the donor and acceptor orbitals as proposed in the Dewar-Chatt-Duncanson model.

Methods

Notation

We adopt the following notation in the subsequent presentation. The initial determinant is I, and the final determinant is F. Latin letters x, y, z are used to denote fragments, letters i, j, k are used to label occupied molecular orbitals, letters a, b, c are used to label virtual molecular orbitals, and we denote molecular orbitals as $|\psi\rangle$. o and v refer to the total number of occupied and virtual MOs, respectively, while n refers to the total number of MOs. The occupied MO overlap matrix is defined as $(\sigma_o)_{xi,yj} = \langle \psi_{xi} | \psi_{yj} \rangle$, and the virtual MO overlap matrix is defined as $(\sigma_v)_{xa,yb} = \langle \psi_{xa} | \psi_{yb} \rangle$. Since the ALMOs from one fragment are not guaranteed to be orthogonal to those from another fragment, we also need the biorthogonal ALMO basis functions $^{45} |\psi^{xi}\rangle$ and $|\psi^{xa}\rangle$ for the occupied and virtual ALMOs respectively,

which are defined as

$$|\psi^{xi}\rangle = \sum_{yj}^{o} (\sigma_o^{-1})_{yj,xi} |\psi_{yj}\rangle \tag{2}$$

$$|\psi^{xa}\rangle = \sum_{yb}^{v} (\sigma_v^{-1})_{yb,xa} |\psi_{yb}\rangle. \tag{3}$$

With the help of the biorthogonal MOs, the projector onto the occupied subspace can be written as

$$\hat{R} = \sum_{xi}^{o} |\psi_{xi}\rangle\langle\psi^{xi}| = \sum_{xi,yj}^{o} |\psi_{xi}\rangle(\sigma_o^{-1})_{yj,xi}\langle\psi_{yj}|. \tag{4}$$

Similarly, the projector on to the virtual space can be written as

$$\hat{Q} = \hat{1} - \hat{R} = \sum_{xa}^{v} |\psi_{xa}\rangle\langle\psi^{xa}| = \sum_{xa,yb}^{v} |\psi_{xa}\rangle(\sigma_v^{-1})_{yb,xa}\langle\psi_{yb}|$$
 (5)

In this paper, we assume real orbitals for the calculations and construction of the OVOCVs.

Construction of the COVPs

A detailed description of the construction of COVPs was given in our previous work. ¹⁶ To make the paper self-contained, we summarize the main results to enable comparison with the OVOCVs (and NOCVs). We assume both the initial electronic state I and final state F are described by SCF wavefunctions. Specifically, for the CT process in ALMO-EDA, ⁸ I is the CT-free POL state, obtained from SCF for molecular interactions (SCF-MI), ^{34,35} where the MO coefficient matrix is constrained to be block-diagonal. The final state F is unconstrained SCF (includes CT). The energy difference between these two states and the

amount of transferred charge can then be exactly decomposed as

$$\Delta E = 2 \operatorname{Tr} \left\{ \hat{F}_{vo}^{\text{eff}} \hat{X}_{ov} \right\} = \sum_{xy}^{N_{\text{frgm}}} 2 \sum_{i}^{o_{x}} \sum_{a}^{v_{y}} \operatorname{Tr} \left\{ \langle \psi^{ya} | \hat{F}_{vo}^{\text{eff}} | \psi_{xi} \rangle \langle \psi^{xi} | \hat{X}_{ov} | \psi_{ya} \rangle \right\} = \sum_{xy} \Delta E_{x \to y} \quad (6)$$

$$\Delta Q = 2 \operatorname{Tr} \left\{ \hat{P}_{vo}^{\text{eff}} \hat{X}_{ov} \right\} = \sum_{xy}^{N_{\text{frgm}}} 2 \sum_{i}^{o_{x}} \sum_{a}^{v_{y}} \operatorname{Tr} \left\{ \langle \psi^{ya} | \hat{P}_{vo}^{\text{eff}} | \psi_{xi} \rangle \langle \psi^{xi} | \hat{X}_{ov} | \psi_{ya} \rangle \right\} = \sum_{xy} \Delta Q_{x \to y}, \quad (7)$$

where $\hat{F}_{vo}^{\text{eff}}$ and $\hat{P}_{vo}^{\text{eff}}$ are the effective Fock operator and the effective density operator, and \hat{X}_{ov} is the generator of the unitary transformation that connects the initial and final electronic states. Therefore, the energy decrease and the amount of transferred charge associated with electrons moving from fragment x to fragment y is

$$\Delta E_{x \to y} = 2 \sum_{ia} \langle \psi^{ya} | \hat{F}_{vo}^{\text{eff}} | \psi_{xi} \rangle \langle \psi^{xi} | \hat{X}_{ov} | \psi_{ya} \rangle, \tag{8}$$

$$\Delta Q_{x \to y} = 2 \sum_{ia} \langle \psi^{ya} | \hat{P}_{vo}^{\text{eff}} | \psi_{xi} \rangle \langle \psi^{xi} | \hat{X}_{ov} | \psi_{ya} \rangle. \tag{9}$$

We proved that these results remain unchanged under on-fragment unitary transformations of the occupied and virtual orbitals

$$|\psi_{xi}'\rangle = \sum_{xj}^{o_x} U_{xj,xi}^{(x)} |\psi_{xj}\rangle, \tag{10}$$

$$|\psi'_{ya}\rangle = \sum_{yb}^{v_y} U_{yb,ya}^{(y)} |\psi_{yb}\rangle. \tag{11}$$

Therefore, we can choose to use the left and right eigenvectors of the singular value decomposition (SVD) of the interfragment mixing, $\langle \psi^{xi} | \hat{X}_{ov} | \psi_{ya} \rangle$. In this rotated basis, we only need the sum of at most $\min\{o_x, v_y\}$ non-zero terms to describe the energy decrease and the amount of transferred charge. The $\min\{o_x, v_y\}$ pairs of the corresponding occupied and virtual orbitals $\{|\psi'_{xi}\rangle\}$ and $\{|\psi'_{ya}\rangle\}$ obtained in this way are called the complementary occupied-virtual pairs (COVPs), and they give the most compact description of the energy decrease and charge transfer as electrons move from fragment x to fragment y. As discussed

elsewhere, they are particularly useful because typically only one or a few singular values are significant for a given interfragment interaction. ^{15,16}

Construction of the OVOCVs

In the orthonormal basis of occupied and virtual orbitals of initial state I, the matrix representation of \hat{P}_I is

$$P_I = \begin{pmatrix} 1 & 0 \\ 0 & 0 \end{pmatrix} \tag{12}$$

where 1 is $o \times o$ and the diagonal 0 matrix is $v \times v$ in dimension. Under the same basis, the representation of the final density operator P_F can be constructed from P_I as $P_F = \exp\{X\}P_I\exp\{-X\}$, where

$$X = \begin{pmatrix} 0 & X_{ov} \\ -X_{ov}^T & 0 \end{pmatrix} \tag{13}$$

With the SVD of X_{ov} ,

$$X_{ov} = U\Sigma V^T \tag{14}$$

where $\dim(U) = o \times o$, $\dim(\Sigma) = o \times v$, $\dim(V) = v \times v$, we can write ΔP as

$$\Delta P = \begin{pmatrix} U & 0 \\ 0 & V \end{pmatrix} \begin{pmatrix} -\sin^2 \Sigma' & -\cos \Sigma' \sin \Sigma' & 0 \\ -\sin \Sigma' \cos \Sigma' & \sin^2 \Sigma' & 0 \\ 0 & 0 & 0 \end{pmatrix} \begin{pmatrix} U^T & 0 \\ 0 & V^T \end{pmatrix}$$
(15)

where $\Sigma' = \text{diag}(\sigma_1, \sigma_2, ..., \sigma_o)$, and the diagonal 0 matrix is of dimension v - o (assuming o < v, which is the case for most practical calculations).

Since ΔP is rendered diagonal in each of its blocks in the U, V representation, it is natural

to define this choice as the Occupied-Virtual Orbitals for Chemical Valence (OVOCVs).

$$|\phi_{\rm occ}^i\rangle = \sum_k^o U_{ki} |\psi_k\rangle \tag{16}$$

$$|\phi_{\text{vir}}^{i}\rangle = \sum_{a}^{v} V_{ai} |\psi_{a}\rangle, \tag{17}$$

Specifically, $|\phi_{\text{occ}}^i\rangle$ and $|\phi_{\text{vir}}^i\rangle$ are the occupied and virtual orbitals of the *i*th OVOCV pair. Since the OVOCVs are obtained by unitary transformations of an orthonormal basis, they still form an orthonormal basis (with a much smaller dimension, as the virtual orbitals irrelevant to the density deformation are deleted). In the OVOCV basis, ΔP is:

$$\Delta P = \begin{pmatrix} -\sin^2 \Sigma' & -\cos \Sigma' \sin \Sigma' \\ -\sin \Sigma' \cos \Sigma' & \sin^2 \Sigma' \end{pmatrix}$$
 (18)

The (diagonal) oo block is negative semi-definite, corresponding to $\sin^2 \sigma_i$ electron loss from the i^{th} of o initially occupied OVOCV levels. By contrast the (diagonal) vv block is equal and opposite, corresponding to promotion of $\sin^2 \sigma_i$ electrons into the i^{th} of o initially virtual OVOCV levels.

The construction of the OVOCVs is very similar to the definition of the COVPs, except here we used the SVD of X_{ov} in the full occupied and virtual spaces instead of just within each fragment pair of occupied and virtual spaces. In addition, we get agreement on the total amount of transferred charge with the ALMO-EDA definition¹⁶

$$\Delta Q_{\text{OVOCV}} = \sum_{i}^{o} \sin^2 \sigma_i = \Delta Q_{\text{ALMO}}$$
 (19)

Comparison with the NOCVs

NOCV²² orbitals $|\varphi_i\rangle$ are the eigenvectors of the density difference operator $\Delta \hat{P}$, and they provide a decomposition of $\Delta \hat{P}$ as

$$\Delta \hat{P} = \sum_{i}^{o} \lambda_{i} (|\varphi_{i}\rangle\langle\varphi_{i}| - |\varphi_{-i}\rangle\langle\varphi_{-i}|), \qquad (20)$$

where $|\varphi_i\rangle$ and $|\varphi_{-i}\rangle$ are NOCVs with paired positive and negative eigenvalues, and we proved that $\lambda_i = \sin \sigma_i$, where σ_i are the diagonal elements of the Σ matrix in Eqn. 14.

By diagonalizing $\Delta \hat{P}$ in the OVOCV basis as shown in Eqn. 18, we can express the NOCVs as a linear combination of the OVOCV orbitals.

$$|\varphi_{\pm i}\rangle = C_{\pm i} \left[|\phi_{\text{occ}}^i\rangle + \frac{-\sin\sigma_i \mp 1}{\cos\sigma_i} |\phi_{\text{vir}}^i\rangle \right]$$
 (21)

with normalization factor $C_{\pm i}^2 = \frac{\cos^2 \sigma_i}{2 \pm 2 \sin \sigma_i}$. Therefore, the density difference operator can be written as

$$\Delta \hat{P} = \sum_{i}^{o} \sin \sigma_{i} (|\varphi_{i}\rangle\langle\varphi_{i}| - |\varphi_{-i}\rangle\langle\varphi_{-i}|)$$

$$= \sum_{i}^{o} \left[\sin^{2} \sigma_{i} (|\phi_{\text{vir}}^{i}\rangle\langle\phi_{\text{vir}}^{i}| - |\phi_{\text{occ}}^{i}\rangle\langle\phi_{\text{occ}}^{i}|) - \sin \sigma_{i} \cos \sigma_{i} (|\phi_{\text{occ}}^{i}\rangle\langle\phi_{\text{vir}}^{i}| + |\phi_{\text{vir}}^{i}\rangle\langle\phi_{\text{occ}}^{i}|) \right]$$
(22)

It will be shown later through examples that the occupied and virtual orbitals of the OVOCVs often show small spatial overlap with each other, such that their products decay exponentially to 0 as the inter-fragment distance increases. If we drop these occupied-virtual product terms in Eqn. 22, we get

$$\Delta \hat{P} = \sum_{i}^{o} \sin \sigma_{i} (|\varphi_{i}\rangle\langle\varphi_{i}| - |\varphi_{-i}\rangle\langle\varphi_{-i}|) \sim \sum_{i}^{o} \sin^{2} \sigma_{i} (|\phi_{\text{vir}}^{i}\rangle\langle\phi_{\text{vir}}^{i}| - |\phi_{\text{occ}}^{i}\rangle\langle\phi_{\text{occ}}^{i}|).$$
 (23)

Therefore, each pair of delocalized NOCVs essentially describes the same charge transfer effect as a pair of more localized OVOCVs. However, the amount of transferred charge

associated with the i^{th} NOCV pair, $\sin \sigma_i$, is well-known to be too large.^{39,42} As already discussed, this is reduced to $\sin^2 \sigma_i$ in the OVOCV picture, which is the same total amount of transferred charge from the COVPs under ALMO-EDA.

Connection to the excitation number

The excitation number 43 was introduced to remedy the fact that one should not interpret the integral of attachment or detachment densities 18 as the number of electrons excited or promoted from an initial state to a final state. When such states are single determinants, a logical alternative is to count the electrons in the final state that did not lie in the initally occupied subspace (or vice-versa). This can be easily accomplished using their idempotent one-particle density operators, \hat{P}_I and \hat{P}_F .

$$\eta = \text{Tr}\Big\{\hat{P}_I - \hat{P}_I\hat{P}_F\hat{P}_I\Big\}$$
(24)

Direct substitution of the definition of $\hat{P} = \sum_i |\psi_i\rangle\langle\psi_i|$ in terms of the occupied MOs, $\{|\psi_i\rangle\}$ (not to be confused with the NOCVs or OVOCVs!) leads to:

$$\eta = o - \sum_{ij} s_{ij}^2 \tag{25}$$

where the overlaps of initial and final occupied MOs define s_{ij} . Alternatively, we can make use of Eq. 24 together with the definition of P_I from Eq. 12 and $P_F = P_I + \Delta P$, where ΔP is given most compactly by Eq. 18. This leads directly to a third equivalent expression for η :

$$\eta = \sum_{i} \sin^2 \sigma_i \equiv \Delta Q_{\text{OVOCV}} \tag{26}$$

This establishes that the OVOCV analysis recovers the excitation number, with the direct benefit of connecting to energy decomposition analysis, as discussed below.

EDA with the OVOCVs

ALMO-OVOCV

The OVOCVs can be used to examine the energy lowering between any initial state i and final state f that are each single determinants. As shown in Eqn. 6, the energy difference ΔE between two states can be written as 16

$$\Delta E = 2 \operatorname{Tr} \left\{ \hat{F}_{vo}^{\text{eff}} \hat{X}_{ov} \right\}. \tag{27}$$

Decomposition of the \hat{X}_{ov} operator in terms of the OVOCVs gives us

$$\hat{X}_{ov} = \sum_{i}^{o} \sigma_{i} |\phi_{\text{occ}}^{i}\rangle\langle\phi_{\text{vir}}^{i}|.$$
(28)

Combining these two equations gives

$$\Delta E = \sum_{i}^{o} 2\sigma_{i} \langle \phi_{\text{vir}}^{i} | \hat{F}_{vo}^{\text{eff}} | \phi_{\text{occ}}^{i} \rangle = \sum_{i}^{o} \Delta E_{i}.$$
 (29)

Therefore, the energy decrease associated with each OVOCV pair is $\Delta E_i = 2\sigma_i \langle \phi_{\rm vir}^i | \hat{F}_{vo}^{\rm eff} | \phi_{\rm occ}^i \rangle$.

ETS-OVOCV

We have shown previously 16 that the energy difference ΔE between any two single determinant states can equally well be written in terms of associated change in density. That is exactly the form used in ETS-NOCV analysis:

$$\Delta E = \text{Tr}\Big\{\hat{F}^{\text{eff}}\Delta\hat{P}\Big\},\tag{30}$$

where \hat{F}^{eff} is an effective fock operator obtained from a linear integration over the density matrices between the two states. Using the decomposition of $\Delta \hat{P}$ in Eqn. 22, we have

$$\Delta E = \sum_{i}^{o} \sin^{2} \sigma_{i} \left(\langle \phi_{\text{vir}}^{i} | \hat{F}^{\text{eff}} | \phi_{\text{vir}}^{i} \rangle - \langle \phi_{\text{occ}}^{i} | \hat{F}^{\text{eff}} | \phi_{\text{occ}}^{i} \rangle \right)$$

$$- \sum_{i}^{o} \sin \sigma_{i} \cos \sigma_{i} \left(\langle \phi_{\text{vir}}^{i} | \hat{F}^{\text{eff}} | \phi_{\text{occ}}^{i} \rangle + \langle \phi_{\text{occ}}^{i} | \hat{F}^{\text{eff}} | \phi_{\text{vir}}^{i} \rangle \right)$$

$$= \sum_{i}^{o} \Delta E_{i}$$
(31)

Therefore, the energy decrease associated with each OVOCV pair is

$$\Delta E_{i} = \sin^{2} \sigma_{i} \left(\langle \phi_{\text{vir}}^{i} | \hat{F}^{\text{eff}} | \phi_{\text{vir}}^{i} \rangle - \langle \phi_{\text{occ}}^{i} | \hat{F}^{\text{eff}} | \phi_{\text{occ}}^{i} \rangle \right) - \sin \sigma_{i} \cos \sigma_{i} \left(\langle \phi_{\text{vir}}^{i} | \hat{F}^{\text{eff}} | \phi_{\text{occ}}^{i} \rangle + \langle \phi_{\text{occ}}^{i} | \hat{F}^{\text{eff}} | \phi_{\text{vir}}^{i} \rangle \right).$$
(32)

This is *exactly* the same as the energy decrease associated with each NOCV pair, but expressed in the OVOCV basis.

Computational details

Isolated fragment SCF calculations were first performed, after which the block diagonal MO coefficient matrix and the density matrix P_{FRZ} of the frozen state were constructed using the occupied orbitals and DQ-FERFs of each fragment. We then ran SCF-MI calculations to obtain the polarized state and the density matrix P_{POL} . The generator \mathbf{X} of the unitary transformation connecting FRZ and POL states was obtained by minimizing the cost function $C = \|P_{\text{POL}} - U(X)P_{\text{FRZ}}U(X)^T\|_F^2$ as in reference 15. For spin-polarized calculations, the above procedures were performed for the α and β spin sectors separately, since the density matrices do not couple orbitals with different spins. A similar procedure connects the POL and FULL states, where the former excludes CT while the latter is fully optimized and thus includes CT.

The OVOCV analysis algorithm was implemented in a development version of the Q-

Chem quantum chemistry program. 47 Unless otherwise specified, the ω B97X-V functional 37 with the def2-TZVPD basis set 48,49 were used for geometry optimization and vibrational mode analysis, and ω B97X-V/def2-TZVPD single point calculations were used for the energy decomposition analysis. Geometries of all molecules were confirmed to be local minima on the potential energy surface by confirming that the Hessian matrix has no negative eigenvalues. All the COVP, NOCV and OVOCV orbitals were plotted with an isosurface value of ± 0.07 a.u. using open source software IQmol. The density difference plots were generated with VMD, 50 where the red region indicates electron density decrease (depletion of electrons) and the blue region indicates electron density increase (accumulation of electrons). The occupied and virtual COVPs and OVOCVs were plotted in transparent solid and wire-frame style respectively, while the NOCVs were plotted in transparent solid style.

Results and discussion

$\mathbf{H}-\mathbf{H}^+$

Let us first consider a simple but illustrative toy example with a hydrogen atom and a proton. In the minimal basis set, we only have two orbitals $|\phi_1\rangle$ and $|\phi_2\rangle$, which are the 1s orbitals located on the H atom and the proton. At moderately large distances, these two orbitals can be regarded as orthogonal. Therefore, the initial state is $|\psi_{\rangle} = |\phi_1\rangle$, and the final state is $|\psi_f\rangle = \frac{1}{\sqrt{2}}(|\phi_1\rangle + |\phi_2\rangle)$. In the $\{|\phi_1\rangle, |\phi_2\rangle\}$ basis, the density operators $\hat{P}_i = |\psi_i\rangle\langle\psi_i|$ and $\hat{P}_f = |\psi_f\rangle\langle\psi_f|$ can be represented as

$$\mathbf{P}_i = \begin{pmatrix} 1 & 0 \\ 0 & 0 \end{pmatrix} \qquad \mathbf{P}_f = \frac{1}{2} \begin{pmatrix} 1 & 1 \\ 1 & 1 \end{pmatrix}. \tag{33}$$

The generator of the unitary transformation mixing the two orbitals is:

$$\mathbf{X} = \begin{pmatrix} 0 & \theta \\ -\theta & 0 \end{pmatrix},\tag{34}$$

and the unitary transformation itself is simply

$$\mathbf{U}(\mathbf{X}) = \exp(\mathbf{X}) = \begin{pmatrix} \cos \theta & \sin \theta \\ -\sin \theta & \cos \theta \end{pmatrix}. \tag{35}$$

Therefore, we have

$$\Delta \mathbf{P} = \mathbf{U}(\mathbf{X})\mathbf{P}_{i}\mathbf{U}(\mathbf{X})^{T} - \mathbf{P}_{i} = \begin{pmatrix} 1 & 0 \\ 0 & 1 \end{pmatrix} \begin{pmatrix} -\sin^{2}\theta & -\sin\theta\cos\theta \\ -\sin\theta\cos\theta & \sin^{2}\theta \end{pmatrix} \begin{pmatrix} 1 & 0 \\ 0 & 1 \end{pmatrix}$$
(36)

By comparing with the representation of $\Delta \mathbf{P}$ from Eqn. 33, we find $\theta = -\frac{\pi}{4}$. Thus, the amount of transferred charge is $\Delta Q_{\text{OVOCV}} = \sin^2 \theta = \frac{1}{2}$, and the occupied and virtual OVOCVs are simply $|\phi_1\rangle$ and $|\phi_2\rangle$. In this case, the OVOCVs are exactly the same as the COVPs, and they also give the correct number of transferred electrons. ¹⁶ By contrast, direct use of the eigenvalues from standard NOCV analysis yields an unphysical value for the charge rearrangment of $\Delta Q_{\text{NOCV}} = \sin \theta = \frac{1}{\sqrt{2}}$.

$$(\mathbf{Me}_2\mathbf{N})_2\mathbf{C} = \mathbf{S}\cdots\mathbf{I}_2$$
 cluster

The complex between tetramethylthiourea and iodine was experimentally characterized⁵¹ as a strong halogen-bonding system whose stability was relatively insensitive to the nature of the solvent. The authors suggested charge transfer was a major contribution to the stability of the complex that led to solvent insensitivity. We investigated this system with EDA to understand the importance and the nature of its charge transfer process. From Table 1, the dispersion energy and polarization energy roughly cancels out the repulsive combination

of electrostatic interaction and Pauli repulsion. The large negative interaction energy is therefore nearly all due to the CT energy.

Table 1: Contributions to the interaction energy (in kJ/mol) and amounts of transferred charge (in me⁻) calculated using ALMO EDA for the $(Me_2N)_2C=S\cdots I_2$ complex at its optimal geometry. $\Delta E_{\rm ele+Pauli}$ is the energy decrease due to electrostatic interaction and Pauli repulsion, and $\Delta E_{\rm disp}$ is the dispersion energy.

$\Delta E_{\text{ele+Pauli}}$	$\Delta E_{\rm disp}$	$\Delta E_{ m POL}$	$\Delta Q_{ m POL}$	$\Delta E_{\rm CT}$	ΔQ_{CT}	$\Delta E_{ m INT}$
73.33	-45.46	-25.18	25.40	-55.19	77.03	-52.51

Table 2 shows the CT decomposition results from the 4 EDA methods. As guaranteed by the formal theory, all 4 methods give the same energy lowering due to CT. However, the amount of transferred charge from ETS-NOCV is unreasonably large $(0.8 e^-)$, while those of the other three methods are the same by construction, and are more than 10 times smaller $(0.08 e^-)$. The energy decrease from the most significant COVP, NOCV and OVOCV pair are roughly the same, and we notice that the results from ALMO-OVOCV and ETS-OVOCV are identical, as established in the Theory section. Likewise the ALMO-COVP charge movement approximately matches that for ALMO-OVOCV, while by construction ALMO-OVOCV matches ETS-OVOCV exactly.

Table 2: Energies (in kJ/mol) and amounts of transferred charge (in me^-) of the CT process for the formation of $(Me_2N)_2C = S \cdots I_2$ complex at its optimal geometry, calculated with ALMO-COVP, ETS-NOCV, ALMO-OVOCV and ETS-OVOCV methods. The most important COVP, NOCV, and OVOCV are also provided as well as their percentage contributions (in the parentheses) to CT energy decrease and the amount of transferred charge.

	$\Delta E_{\rm CT}$	ΔQ_{CT}	$\Delta E_1(\%)$	$\Delta Q_1(\%)$
ALMO-COVP	-55.19	77.03	-46.36(84.0)	72.04(93.5)
ETS-NOCV	-55.20	792.28	-45.39(82.2)	371.26(46.9)
ALMO-OVOCV	-55.19	77.03	-45.86(83.1)	68.92(89.5)
ETS-OVOCV	-55.19	77.03	-45.39(82.2)	68.92(89.5)
				` '

Figure 2 shows that the most significant COVP and OVOCV pair are visually very similar to each other, though they are not guaranteed to be identical. They both show

electron donation from the lone pair of the S of tetramethylthiourea to the σ^* orbital of I₂. The density difference plot of the most important NOCV pair also reveals the same chemistry, but it is less straightforward to recognize the donor and acceptor orbitals, and the NOCVs are not very helpful at all. From the chemical standpoint, with the density functional calculations reported here, the driving force behind this strong halogen bond is the CT process which is dominated by donating roughly 0.07 e^- or 3.5% of the S lone pair of electrons into the I₂ σ^* acceptor orbital, with an associated energy lowering of about 46 kJ/mol.

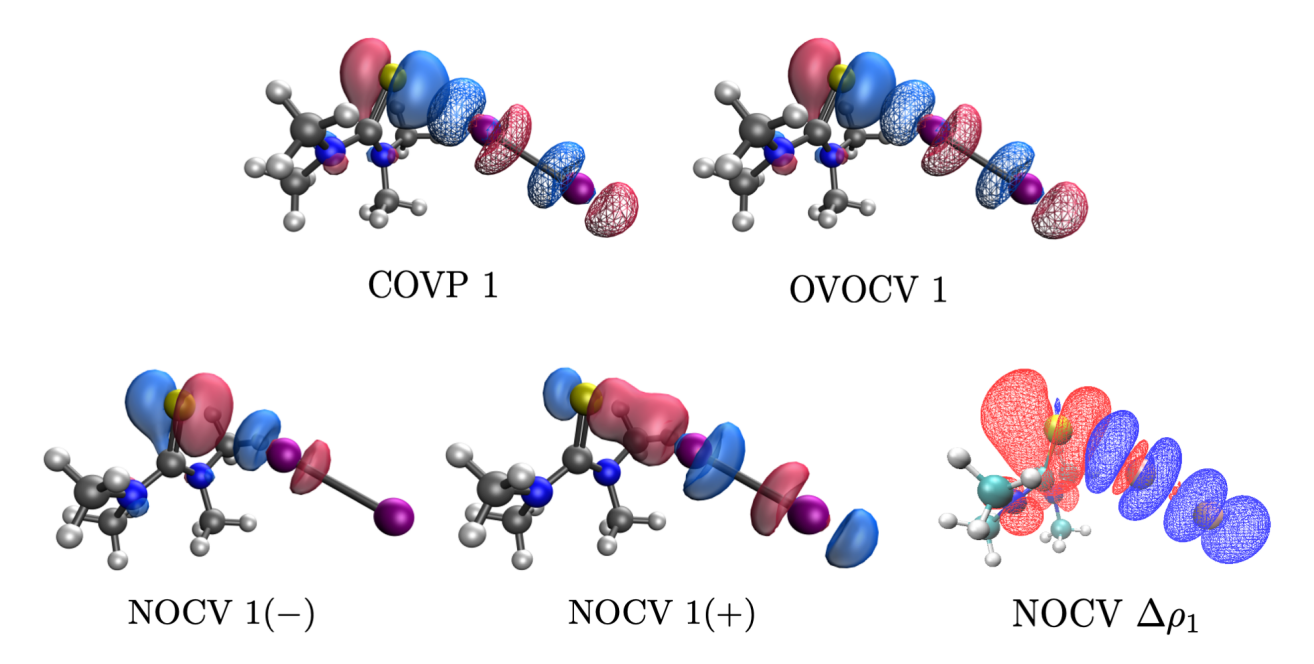


Figure 2: Plots of the most significant COVP, OVOCV, NOCV and associated density difference of the $(Me_2N)_2C = S \cdots I_2$ complex. The NOCV density difference plot is at an isosurface value $\pm 1 \times 10^{-4}$ a.u.

$[\mathbf{PtCl_3}]^- - \mathbf{C_2H_4}$ cluster

Zeise's salt, 52,53 potassium trichloro(ethylene)platinate(II) hydrate with the formula $K[PtCl_3(C_2H_4)]\cdot H_2O$ was one of the first organometallic compounds to be reported. The structure and bonding of its stable anion were a mystery until being explained by the Dewar-Chatt-Duncanson model. 4,5 Here, we revisit this classical system with EDA methods, which

will reveal the exact donor and acceptor orbitals of the Dewar-Chatt-Duncanson model. The Pt atom has square-planar coordination with 3 Cl⁻ ligands. The fourth ligand is ethene which is η^2 coordinated with the π orbital approximately perpendicular to the PtCl₃ plane. For EDA analysis, we shall consider [PtCl₃]⁻ to be one fragment, and C₂H₄ to be the second fragment, and we shall investigate the electron flow between them after first optimizing the polarized state in the usual ALMO-EDA fashion.⁸

The overall EDA picture is given in Table 3, which reveals that $\Delta E_{\rm CT}$ is the critical contributor to formation of the stable [PtCl₃]⁻-C₂H₄ complex. At the stable geometry, the complex is unbound by 180 kJ/mol without considering CT, and then is bound by 230 kJ/mol upon inclusion of CT. We next analyze the CT process using the existing ALMO-COVP and ETS-NOCV methods, as well as the new approaches using OVOCV analysis. Table 4 provides the CT decomposition results from all 4 EDA methods, showing that all 4 methods recover the correct amount of CT energy of -411 kJ/mol at the ω B97X-V/def2-TZVPD level of theory. Both OVOCV methods give the amount of transferred charge of 0.38 e^- , which is exactly the same as the ALMO-COVP method, as explained by our theory. On the other hand, ETS-NOCV gives a much larger and rather unphysical amount of transferred charge totaling 1.9 e^- . COVP, NOCV and OVOCV all reveal 2 significant donor-acceptor pairs, with about 50% and 40% energy contributions to the CT energy decrease.

Table 3: Energies (in kJ/mol) and amounts of transferred charge (in me⁻) calculated using ALMO EDA for the [PtCl₃]⁻-C₂H₄ complex at its optimal geometry. $\Delta E_{\text{ele+Pauli}}$ is the energy decrease due to electrostatic interaction and Pauli repulsion, and ΔE_{disp} is the dispersion energy.

$\Delta E_{\text{ele+Pauli}}$	$\Delta E_{\rm disp}$	$\Delta E_{ m POL}$	ΔQ_{POL}	$\Delta E_{\rm CT}$	ΔQ_{CT}	$\Delta E_{ m INT}$
461.4	-79.2	-201.4	57.2	-410.8	384.7	-230.0

Table 4: Energies (in kJ/mol) and amounts of transferred charge (in me^-) of the CT process for the formation of $[PtCl_3]^--C_2H_4$ cluster at optimal geometry, calculated with ALMO-COVP, ETS-NOCV, ALMO-OVOCV and ETS-OVOCV methods. The most important COVP, NOCV, and OVOCV are also provided as well as their percentage contributions (in the parentheses) to CT energy decrease and the amount of transferred charge.

	ΔE_{CT}	ΔQ_{CT}	$\Delta E_1(\%)$	$\Delta Q_1(\%)$	$\Delta E_2(\%)$	$\Delta Q_2(\%)$
ALMO-COVP	-410.8	384.7	-202.0(49.2)	169.3(44.0)	-163.1(39.7)	205.6(53.4)
ETS-NOCV	-410.9	1876.4	-211.6(51.5)	598.1(31.9)	-161.8(39.4)	615.5(32.8)
ALMO-OVOCV	-410.8	384.7	-211.1(51.4)	178.8(46.5)	-162.4(39.5)	189.4(49.2)
ETS-OVOCV	-410.8	384.7	-211.6(51.5)	178.8(46.5)	-161.8(39.4)	189.4(49.2)

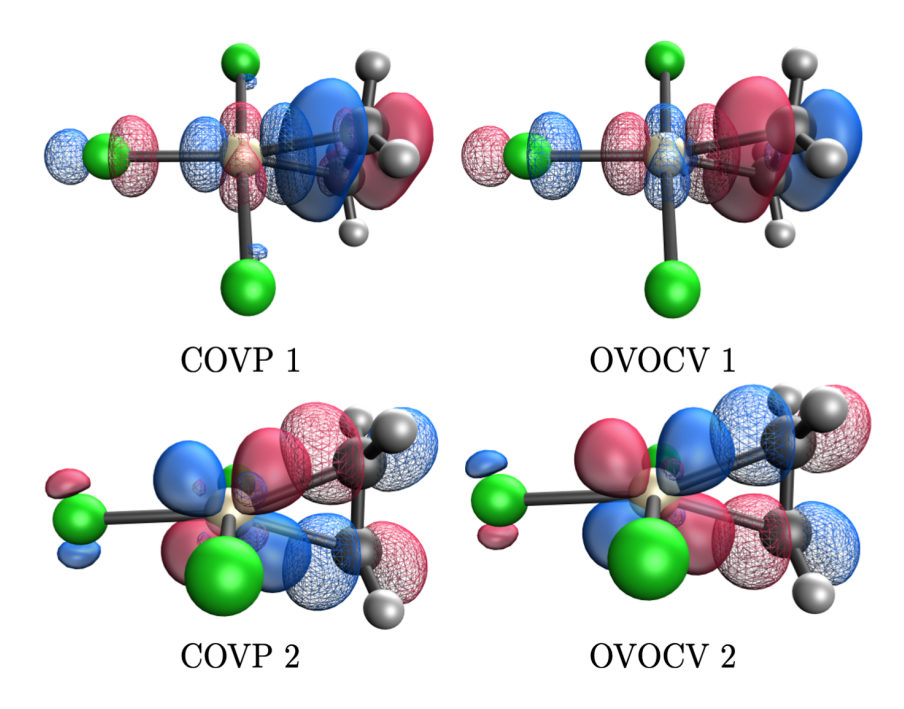


Figure 3: Plots of the most significant COVP and OVOCV of the $[PtCl_3]^- - C_2H_4$ cluster.

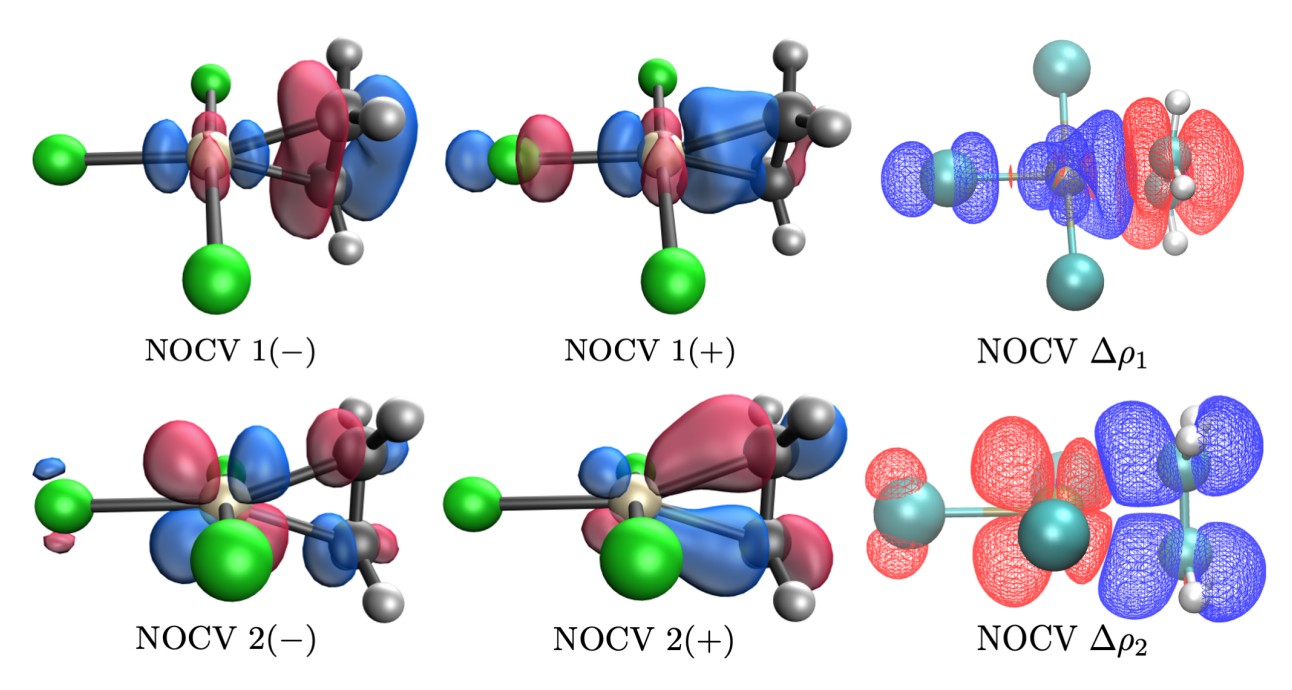


Figure 4: Plots of the most significant NOCV and associated density difference of the $[PtCl_3]^--C_2H_4$ cluster. The NOCV density difference plot is at isosurface value $\pm 5 \times 10^{-4}$ a.u.

Figure 3 shows the most significant COVP and OVOCV. It is clear that the most significant COVP and OVOCV pairs look very similar to each other. The largest contribution describes forward electron donation from the π HOMO of ethylene to the $5d_{x^2-y^2}$ orbital of Pt (accounting for 50% of the CT energy). Only slightly smaller is back-donation from the $5d_{xz}$ orbital of Pt to the π^* LUMO of ethylene (accounting for 40% of the CT energy). These two donor-acceptor pairs beautifully create the donation and back-donation processes of the Dewar-Chatt-Duncanson model without any assumptions.

The spatial separation between the occupied and virtual orbitals of OVOCV is obvious, which results in a small occupied-virtual overlap and makes Eqn. 23 an excellent approximation. However, it is worth noting that such a strong resemblance between COVP and OVOCV is not guaranteed, since the OVOCV are generated by mixing the total occupied space and total virtual space separately, without any use of fragments (apart from generating the initial polarized state). It is a striking proof of usefulness to see that the OVOCVs are mostly separated by fragments. In contrast, the COVPs always preserve the nice fea-

ture of fragment-localised occupied and virtual orbitals (except for some small delocalized orthogonalization tails) due to the fragment-wise projections of the occupied and virtual spaces.

Figure 4 shows that the density difference plots of the most important NOCV pairs basically tells the same chemical story. However, it is a bit harder to recognize the involved orbitals, as the signs of the lobes cannot be represented, and the thorough diagonalization of $\Delta \hat{P}$ mixes the occupied space and the virtual space, which makes the resulting orbitals more distorted. This is very clear from the delocalized character of the NOCV orbitals.

$$(Cp)_3La\cdots(C \equiv NCy)$$
 complex

In a previous study of the tris(cyclopentadienyl)-cyclohexylisonitrile complexes of trivalent actinide and lanthanide metal cations, 54 it was claimed that the lanthanide and actinide cations have different bonding interactions with the isonitrile group. While the bonding of actinides is dominated by strong An \rightarrow C \equiv NCy π back-donation, there is little Ln \rightarrow C \equiv NCy π back-donation. Instead, the lanthanide-isonitrile interaction is mainly due to a strong σ donation from the isonitrile carbon lone pair into the $5d_{z^2}$ orbital of the lanthanide. Here, we study the bonding interaction of the Cp₃ La····C \equiv NCy complex to explore this binding interaction using the OVOCV analysis, and the def2 effective core potential (ECP) 55,56 was used to account for relativistic effects and to simplify the calculation. From Table 5, the combination of electrostatic, Pauli repulsion, dispersion and polarization energy is roughly the same as the CT energy, which indicates the importance of CT in the bond formation.

Table 5: Contributions to the interaction energy (in kJ/mol) and amounts of transferred charge (in me⁻) calculated using ALMO EDA for the Cp₃ La···C \equiv NCy complex at its optimal geometry. $\Delta E_{\rm ele+Pauli}$ is the energy decrease due to electrostatic interaction and Pauli repulsion, and $\Delta E_{\rm disp}$ is the dispersion energy.

$\Delta E_{\text{ele+Pauli}}$	$\Delta E_{\rm disp}$	$\Delta E_{ m POL}$	ΔQ_{POL}	ΔE_{CT}	ΔQ_{CT}	$\Delta E_{ m INT}$
22.00	-44.55	-26.91	14.72	-39.59	27.41	-89.04

Table 6 shows the CT decomposition results from the 4 EDA methods. As guaranteed by the formal theory, all 4 methods give the same energy lowering due to CT. However, the amount of transferred charge from the ETS-NOCV eigenvalues is unreasonably large (0.56 e^-) and is 20 times larger than those of the other three methods (0.027 e^-). The energy decrease from the most significant COVP, NOCV and OVOCV pair are roughly the same, and we notice that the results from ALMO-OVOCV and ETS-OVOCV are identical, as established in the Methods section. Likewise the ALMO-COVP charge movement approximately matches that for ALMO-OVOCV, while by construction ALMO-OVOCV matches ETS-OVOCV exactly. In addition, all the methods show a dominant orbital interaction which contributes 80% of the CT energy.

Table 6: Energies (in kJ/mol) and amounts of transferred charge (in me^-) of the CT process for the formation of $(Cp)_3La\cdots(C \equiv NCy)$ complex at its optimal geometry, calculated with ALMO-COVP, ETS-NOCV, ALMO-OVOCV and ETS-OVOCV methods. The most important COVP, NOCV, and OVOCV are also provided as well as their percentage contributions (in the parentheses) to CT energy decrease and the amount of transferred charge.

	ΔE_{CT}	ΔQ_{CT}	$\Delta E_1(\%)$	$\Delta Q_1(\%)$
ALMO-COVP	-39.58	27.41	-29.95(75.7)	22.10(80.6)
ETS-NOCV	-39.59	567.89	-31.64(79.9)	197.40(34.8)
ALMO-OVOCV	-39.58	27.41	-31.67(80.0)	19.48(71.1)
ETS-OVOCV	-39.58	27.41	-31.63(79.9)	19.48(71.1)

Figure 5 shows that the most significant COVP and OVOCV pair are visually very similar to each other, though the COVP virtual orbital has a small delocalized orthogonalization tail. They both clearly show the electron donation from the lone pair of the C of isonitrile group to the $5d_{z^2}$ orbital of La³⁺. The density difference plot of the most important NOCV pair also reveals the same chemistry, but it is less straightforward to recognize the donor and acceptor orbitals due to a lack of the phase information, and the NOCVs are not very helpful at all, as they are mixtures of the donor and acceptor orbitals. Back-donation is indeed very secondary in this interaction.

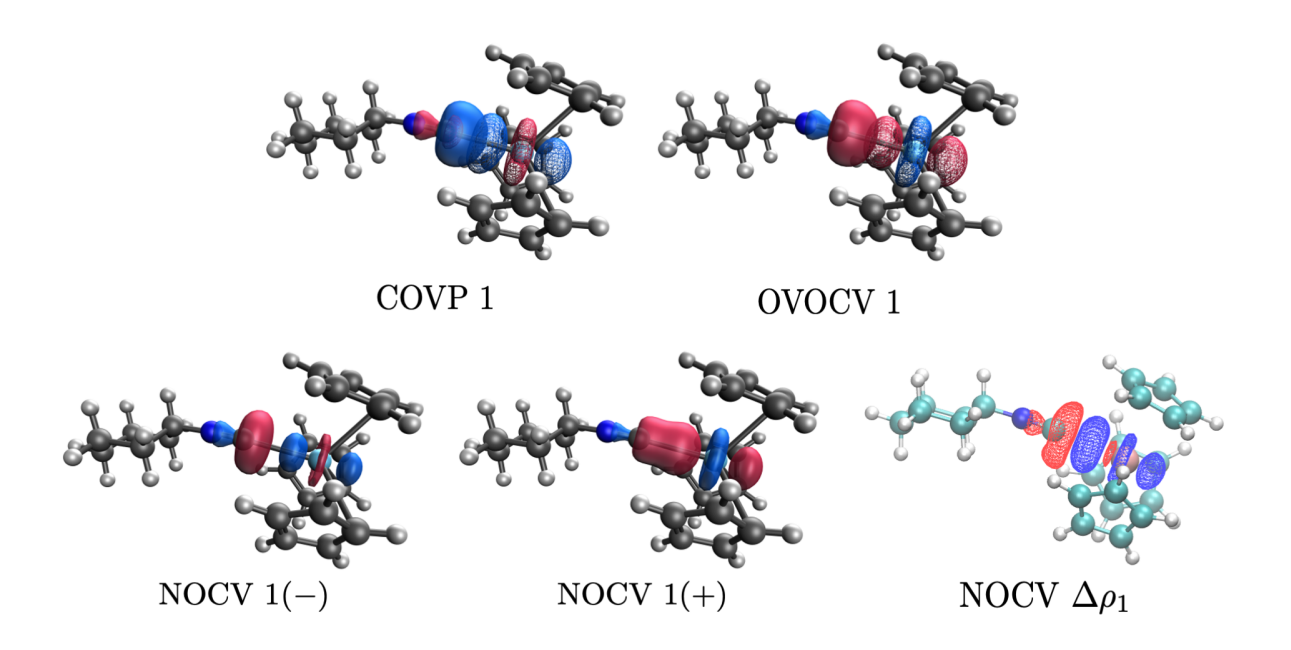


Figure 5: Plots of the most significant COVP, OVOCV, NOCV and associated density difference of the $Cp_3 La \cdots C \equiv NCy$ complex. The NOCV density difference plot is at an isosurface value $\pm 3 \times 10^{-4}$ a.u.

Conclusions

In this work, we have introduced a new way of analyzing the change in density that occurs when electron delocalization occurs in the formation of molecular complexes and/or bonds. More generally, the same analysis can be used to connect any initial determinant to any final determinant for a given molecular geometry and choice of atomic orbital basis set.

We have defined occupied-virtual orbitals for chemical valence (OVOCVs) to be paired sets of occupied and virtual orbitals that most compactly describe the delocalization process (or the change in density) through singular values that are identical to those that enter the popular natural orbitals for chemical valence (NOCV) analysis.

Our main conclusions are:

1. The OVOCVs provide a clear picture of electron promotion from initially filled orbitals

(the occupied level of a given OVOCV pair) to initially empty orbitals (the virtual level of the same OVOCV pair). By contrast NOCVs mix occupieds and virtuals.

- 2. The number of electrons *promoted* in the OVOCV analysis is reasonable and exactly matches that obtained by the existing complementary occupied-virtual orbital pair (COVP) analysis. By contrast the number of electrons *rearranged* in the NOCV analysis is much too large: actually the square root of the OVOCV value for each pair.
- 3. The number of electrons promoted to connect the initial state to the final state is proved to be identical to the excitation number defined independently. The number of electrons rearranged in NOCV analysis is identical to that obtained by integrating the attachment or detachment densities.
- 4. The OVOCV analysis can be used to replace or complement NOCV analysis in an energy decomposition analysis such as the extended transition state (ETS)-NOCV scheme. The energy contributions are identical, and one gains the advantages listed above for the orbital character, and the number of electrons promoted or delocalized.
- 5. We illustrated these considerations with the model problem of electron transfer from H to H⁺ to form stretched H_2^+ as well as more chemically realistic examples of a strong halogen bond between tetramethylthiourea and iodine, the synergic η^2 coordination bonding between C_2H_4 and $[PtCl_3]^-$ in Zeise's salt, and binding in the Cp_3 La···· $C \equiv NCy$ complex.

Conflicts of Interest

MH-G is a part-owner of Q-Chem Inc, whose software was used for all developments and calculations reported here.

Acknowledgements

This work was supported by the U.S. National Science Foundation through Grant No. CHE-2313791, and additional support from CALSOLV.

References

- (1) Lewis, G. N. Valence and the Structure of Atoms and Molecules; Chemical Catalog Company, Incorporated, 1923.
- (2) Jensen, W. B. The Lewis acid-base definitions: a status report. Chem. Rev. 1978, 78, 1–22.
- (3) Sidgwick, N. V. The electronic theory of valency; Clarendon Press, 1927.
- (4) Dewar, J. A review of the pi-complex theory. Bull. Soc. Chim. Fr. 1951, 18, C71–C79.
- (5) Chatt, J.; Duncanson, L. 586. Olefin co-ordination compounds. Part III. Infra-red spectra and structure: attempted preparation of acetylene complexes. J. Chem. Soc. (Resumed) 1953, 2939–2947.
- (6) Blyholder, G. Molecular orbital view of chemisorbed carbon monoxide. J. Phys. Chem. 1964, 68, 2772–2777.
- (7) Zhao, L.; Hermann, M.; Schwarz, W. E.; Frenking, G. The Lewis electron-pair bonding model: modern energy decomposition analysis. *Nat. Rev. Chem.* **2019**, *3*, 48–63.
- (8) Mao, Y.; Loipersberger, M.; Horn, P. R.; Das, A.; Demerdash, O.; Levine, D. S.; Veccham, S. P.; Head-Gordon, T.; Head-Gordon, M. From intermolecular interaction energies and observable shifts to component contributions and back again: A tale of variational energy decomposition analysis. *Annu. Rev. Phys. Chem.* 2021, 72, 641–666.
- (9) Bickelhaupt, F. M.; Guerra, C. F.; Mitoraj, M.; Sagan, F.; Michalak, A.; Pan, S.; Frenking, G. Clarifying notes on the bonding analysis adopted by the energy decomposition analysis. *Phys. Chem. Chem. Phys.* 2022, 24, 15726–15735.

- (10) Reed, A. E.; Curtiss, L. A.; Weinhold, F. Intermolecular interactions from a natural bond orbital, donor-acceptor viewpoint. *Chem. Rev.* **1988**, *88*, 899–926.
- (11) Weinhold, F.; Landis, C. R. Valency and bonding: a natural bond orbital donor-acceptor perspective; Cambridge University Press, 2005.
- (12) Mitoraj, M.; Michalak, A. Natural orbitals for chemical valence as descriptors of chemical bonding in transition metal complexes. *J. Mol. Model.* **2007**, *13*, 347–355.
- (13) Michalak, A.; Mitoraj, M.; Ziegler, T. Bond orbitals from chemical valence theory. *J. Phys. Chem. A* **2008**, *112*, 1933–1939.
- (14) Khaliullin, R. Z.; Bell, A. T.; Head-Gordon, M. Analysis of charge transfer effects in molecular complexes based on absolutely localized molecular orbitals. *J. Chem. Phys.* **2008**, *128*, 184112.
- (15) Veccham, S. P.; Lee, J.; Mao, Y.; Horn, P. R.; Head-Gordon, M. A non-perturbative pairwise-additive analysis of charge transfer contributions to intermolecular interaction energies. *Phys. Chem. Chem. Phys.* 2021, 23, 928–943.
- (16) Shen, H.; Wang, Z.; Head-Gordon, M. Generalization of ETS-NOCV and ALMO-COVP Energy Decomposition Analysis to Connect Any Two Electronic States and Comparative Assessment. J. Chem. Theory Comput. 2022, 18, 7428–7441.
- (17) Martin, R. L. Natural transition orbitals. J. Chem. Phys. 2003, 118, 4775–4777.
- (18) Head-Gordon, M.; Grana, A. M.; Maurice, D.; White, C. A. Analysis of electronic transitions as the difference of electron attachment and detachment densities. *J. Phys. Chem.* **1995**, *99*, 14261–14270.
- (19) Ziegler, T.; Rauk, A. On the calculation of bonding energies by the Hartree Fock Slater method. *Theor. Chim. Acta* **1977**, *46*, 1–10.
- (20) Ziegler, T.; Rauk, A. A Theoretical Study of the Ethylene-Metal Bond in Complexes between Cu⁺, Ag⁺, Pt⁰, or Pt²⁺ and Ethylene, Based on Hartree-Fock-Slater Transition-State Method. *Inorg. Chem.* 1979, 18, 1558–1565.

- (21) Ziegler, T.; Rauk, A. Carbon monoxide, carbon monosulfide, molecular nitrogen, phosphorus trifluoride, and methyl isocyanide as. sigma. donors and. pi. acceptors. A theoretical study by the Hartree-Fock-Slater transition-state method. *Inorg. Chem.* **1979**, *18*, 1755–1759.
- (22) Mitoraj, M. P.; Michalak, A.; Ziegler, T. A combined charge and energy decomposition scheme for bond analysis. J. Chem. Theory Comput. 2009, 5, 962–975.
- (23) Mitoraj, M.; Michalak, A. Donor–acceptor properties of ligands from the natural orbitals for chemical valence. *Organometallics* **2007**, *26*, 6576–6580.
- (24) Frenking, G.; Wichmann, K.; Fröhlich, N.; Loschen, C.; Lein, M.; Frunzke, J.; Rayón, V. M. Towards a rigorously defined quantum chemical analysis of the chemical bond in donor–acceptor complexes. *Coord. Chem. Rev.* **2003**, *238*, 55–82.
- (25) Ndambuki, S.; Ziegler, T. An analysis of unsupported triple and quadruple metal–metal bonds between two homonuclear group 6 transition elements based on the combined natural orbitals for chemical valence and extended transition state method. *Int. J. Quantum Chem.* **2013**, 113, 753–761.
- (26) Mitoraj, M. P.; Kurczab, R.; Boczar, M.; Michalak, A. Theoretical description of hydrogen bonding in oxalic acid dimer and trimer based on the combined extended-transition-state energy decomposition analysis and natural orbitals for chemical valence (ETS-NOCV). J. Mol. Model. 2010, 16, 1789–1795.
- (27) Kurczab, R.; Mitoraj, M. P.; Michalak, A.; Ziegler, T. Theoretical analysis of the resonance assisted hydrogen bond based on the combined extended transition state method and natural orbitals for chemical valence scheme. *J. Phys. Chem. A* **2010**, *114*, 8581–8590.
- (28) Mitoraj, M. P.; Michalak, A. Theoretical description of halogen bonding—an insight based on the natural orbitals for chemical valence combined with the extended-transition-state method (ETS-NOCV). J. Mol. Model. 2013, 19, 4681–4688.
- (29) Mitoraj, M. P.; Michalak, A. Multiple boron-boron bonds in neutral molecules: an insight

- from the extended transition state method and the natural orbitals for chemical valence scheme. *Inorg. Chem.* **2011**, *50*, 2168–2174.
- (30) Mitoraj, M. P.; Parafiniuk, M.; Srebro, M.; Handzlik, M.; Buczek, A.; Michalak, A. Applications of the ETS-NOCV method in descriptions of chemical reactions. J. Mol. Model. 2011, 17, 2337–2352.
- (31) Talaga, P.; Brela, M. Z.; Michalak, A. ETS-NOCV decomposition of the reaction force for double-proton transfer in formamide-derived systems. *J. Mol. Model.* **2018**, *24*, 1–10.
- (32) Díaz, S.; Brela, M. Z.; Gutiérrez-Oliva, S.; Toro-Labbé, A.; Michalak, A. ETS-NOCV Decomposition of the Reaction Force: The HCN/CNH Isomerization Reaction Assisted by Water. J. Comput. Chem. 2017, 38, 2076–2087.
- (33) Sorbelli, D.; Belanzoni, P.; Belpassi, L.; Lee, J.-W.; Ciancaleoni, G. An ETS-NOCV-based computational strategies for the characterization of concerted transition states involving CO2.

 J. Comput. Chem. 2022, 43, 717–727.
- (34) Khaliullin, R. Z.; Head-Gordon, M.; Bell, A. T. An efficient self-consistent field method for large systems of weakly interacting components. *J. Chem. Phys.* **2006**, *124*, 204105.
- (35) Horn, P. R.; Sundstrom, E. J.; Baker, T. A.; Head-Gordon, M. Unrestricted absolutely localized molecular orbitals for energy decomposition analysis: theory and applications to intermolecular interactions involving radicals. *J. Chem. Phys.* **2013**, *138*, 134119.
- (36) Horn, P. R.; Mao, Y.; Head-Gordon, M. Probing non-covalent interactions with a second generation energy decomposition analysis using absolutely localized molecular orbitals. *Phys. Chem. Chem. Phys.* 2016, 18, 23067–23079.
- (37) Chai, J.-D.; Head-Gordon, M. Long-range corrected hybrid density functionals with damped atom-atom dispersion corrections. *Phys. Chem. Chem. Phys.* **2008**, *10*, 6615–6620.
- (38) Dunning Jr, T. H. Gaussian basis sets for use in correlated molecular calculations. I. The atoms boron through neon and hydrogen. *The Journal of chemical physics* **1989**, *90*, 1007–1023.

- (39) Ronca, E.; Belpassi, L.; Tarantelli, F. A quantitative view of charge transfer in the hydrogen bond: the water dimer case. *ChemPhysChem* **2014**, *15*, 2682–2687.
- (40) Pálinkás, N.; Kollár, L.; Kégl, T. Nature of the Metal-Ligand Interactions in Complexes M (PH3) 2 (η2-L)(M= Ni, Pd, Pt; L= CO2, COS, CS2): A Theoretical Study. ChemistrySelect 2017, 2, 5740–5750.
- (41) Papp, T.; Kollár, L.; Kégl, T. Theoretical insights into the nature of Pt-Sn bond: Reevaluating the bonding/back-bonding properties of trichlorostannate with comparison to the cyano ligand. J. Comput. Chem. 2017, 38, 1712–1726.
- (42) Bistoni, G.; Belpassi, L.; Tarantelli, F. Advances in charge displacement analysis. *J. Chem. Theory Comput.* **2016**, *12*, 1236–1244.
- (43) Barca, G. M. J.; Gilbert, A. T. B.; Gill, P. M. W. Excitation number: Characterizing multiply excited states. *J. Chem. Theory Comput.* **2018**, *14*, 9–13.
- (44) Shen, H.; Veccham, S. P.; Head-Gordon, M. Exactly Fragment Additive Breakdown of Polarization for Energy Decomposition Analysis Based on the Self-Consistent Field for Molecular Interactions. J. Chem. Theory Comput. 2023, 19, 8624–8638.
- (45) Head-Gordon, M.; Maslen, P. E.; White, C. A. A tensor formulation of many-electron theory in a nonorthogonal single-particle basis. *J. Chem. Phys.* **1998**, *108*, 616–625.
- (46) Horn, P. R.; Head-Gordon, M. Polarization contributions to intermolecular interactions revisited with fragment electric-field response functions. *J. Chem. Phys.* **2015**, *143*, 114111.
- (47) Epifanovsky, E.; Gilbert, A. T.; Feng, X.; Lee, J.; Mao, Y.; Mardirossian, N.; Pokhilko, P.; White, A. F.; Coons, M. P.; Dempwolff, A. L. et al. Software for the frontiers of quantum chemistry: An overview of developments in the Q-Chem 5 package. J. Chem. Phys. 2021, 155, 084801.
- (48) Weigend, F.; Ahlrichs, R. Balanced basis sets of split valence, triple zeta valence and quadruple zeta valence quality for H to Rn: Design and assessment of accuracy. *Phys. Chem. Chem. Phys.* **2005**, *7*, 3297.

- (49) Rappoport, D.; Furche, F. Property-optimized Gaussian basis sets for molecular response calculations. *J. Chem. Phys.* **2010**, *133*, 134105.
- (50) Humphrey, W.; Dalke, A.; Schulten, K. VMD: visual molecular dynamics. J. Mol. Graphics 1996, 14, 33–38.
- (51) Robertson, C. C.; Perutz, R. N.; Brammer, L.; Hunter, C. A. A solvent-resistant halogen bond. *Chem. Sci.* **2014**, *5*, 4179–4183.
- (52) Zeise, W. C. Von der Wirkung zwischen Platinchlorid und Alkohol, und von den dabei entstehenden neuen Substanzen. *Ann. Phys.* **1831**, *97*, 497–541.
- (53) Hunt, L. The first organometallic compounds. Platinum Met. Rev. 1984, 28, 76–83.
- (54) Kovács, A.; Apostolidis, C.; Walter, O. Competing Metal-Ligand Interactions in Tris (cyclopentadienyl)-cyclohexylisonitrile Complexes of Trivalent Actinides and Lanthanides. Molecules 2022, 27, 3811.
- (55) Dolg, M.; Stoll, H.; Savin, A.; Preuss, H. Energy-adjusted pseudopotentials for the rare earth elements. *Theor. Chim. Acta* **1989**, *75*, 173–194.
- (56) Dolg, M.; Stoll, H.; Preuss, H. A combination of quasirelativistic pseudopotential and ligand field calculations for lanthanoid compounds. *Theor. Chim. Acta* **1993**, *85*, 441–450.

TOC Graphic

